Journal of NeuroVirology, 13: 107–117, 2007

ISSN: 1355-0284 print / 1538-2443 online
DOI: 10.1080/13550280601178226

informa
healthcare

Proteomic profiling reveals that rabies virus infection results in differential expression of host proteins involved in ion homeostasis and synaptic physiology in the central nervous system

Vikas Dhingra,[1] Xiaqing Li,[1] Yuru Liu,[1] and Zhen F Fu[1,2]

[1]*Department of Pathology and* [2]*Department of Infectious Diseases, University of Georgia, Athens, Georgia, USA*

To understand how rabies virus (RV) infection results in neuronal dysfunction, the authors employed proteomics technology to profile host responses to RV infection. In mice infected with wild-type (wt) RV, the expression of proteins involved in ion homeostasis was altered. H^+ ATPase and Na^+/K^+ ATPase were up-regulated whereas Ca^{2+} ATPase was down-regulated, which resulted in reduction of the intracellular Na^+ and Ca^{2+} concentrations. Furthermore, infection with wt RV resulted in down-regulation of soluble NSF attachment receptor proteins (SNAREs) such as α-synaptosome-associated protein (SNAP), tripartite motif-containing 9 (TRIM9), syntaxin, and pallidin, all of which are involved in docking and fusion of synaptic vesicles to and with presynaptic membrane. As a consequence, accumulation of synaptic vesicles was observed in the presynapses of mice infected with wt RV. These data demonstrate that infection with wt RV results in alteration of host protein expression, particularly those involved in ion homeostasis and docking and fusion of synaptic vesicles to presynaptic membrane, which may lead to neuronal dysfunction. On the other hand, attenuated RV up-regulated the expression of proteins involved in the induction of apoptosis, explaining why apoptosis is observed only in cells or animals infected with attenuated RV in previous studies. *Journal of NeuroVirology* (2007) **13,** 107–117.

Keywords: neuronal dysfunction; neurotransmission; pathogenesis; proteomics; rabies virus

Introduction

Despite the fact that rabies is one of the oldest known human infections, the pathogenic mechanism by which rabies virus (RV) infection leads to the development of neurological diseases and death is not well understood (Dietzschold *et al*, 1996). At the bite site, RV enters the peripheral nervous system by binding to specific neural receptors (Lentz *et al*, 1982; Thoulouze *et al*, 1998; Tuffereau *et al*, 1998) with or without local replication (Murphy and Bauer, 1974; Shankar *et al*, 1991). RV spreads by retrograde transport from the periphery to the central nervous system (CNS) (Etessami *et al*, 2000; Jackson, 2003). Rabies patients develop severe agitation, hydrophobia, and paralysis followed by impaired consciousness and coma (Hemachudha, 1994). Patients eventually die of circulatory insufficiency, cardiac arrest, and respiratory failure (Hemachudha, 1994; Tirawatnpong *et al*, 1989). Despite the dramatic and severe clinical course, there are scarce pathological lesions at postmortem examination (Iwasaki and Tobita, 2002; Murphy, 1977). Inflammatory reactions

Address correspondence to Zhen F. Fu, Department of Pathology, College of Veterinary Medicine, University of Georgia, 501 D.W. Brooks Drive, Athens, GA 30602, USA. E-mail: zhenfu@vet.uga.edu

This work is supported partially by Public Health Service grant AI-051560 from the National Institute of Allergy and Infectious Diseases. The authors thank Luciana Sarmento for animal care and infection, Tesfai Tseggai for preparing BSR cells, and Mary Ard for help in electron microscopy. The authors express their gratitude to Dr. John Wagner, Department of Physiology and Toxicology, College of Veterinary Medicine, for critically reviewing this article.

Received 11 September 2006; revised 15 November 2006; accepted 5 December 2006.

are mild with relatively little neuronal degeneration (Murphy, 1977). On the other hand, neuronal dysfunction has been reported in RV infections. Electroencephalographic (EEG) abnormalities have been recorded in mice infected with fixed as well as street RV (Gourmelon *et al*, 1991; Gourmelon *et al*, 1986). Brain electrical activity terminated about 30 min before cardiac arrest, indicating that cerebral death in experimental rabies occurs prior to failure of vegetative functions. Recently, electrophysiological changes have also been observed in human rabies patients (Juntrakul *et al*, 2005; Mitrabhakdi *et al*, 2005). These alterations in neurophysiology could be due to malfunction in neurotransmission. The dynamics of neurotransmission essentially involves four steps, namely, synthesis, storage, release, and uptake (Muller and Nistico, 1988). Decreased binding of neurotransmitters to their receptors have been reported in RV-infected mouse brain, for example, tritiated quinuclinidinyl benzylate binding to acetylcholine (Tsiang, 1982) and serotonin binding to its receptor (Ceccaldi *et al*, 1993). Furthermore, both release and uptake have been found to be reduced for γ-aminobutyric acid (GABA) (Ladogana *et al*, 1994). It was also found that release of norepinephrine (NE), dopamine (DA), dihydroxyphenylacetic acid (DOPAC), serotonin (5-HT), and 5-hydroxyindoleacetic acid (5-HIAA) was reduced at the terminal stage of the disease (Fu and Jackson, 2005). All these results support the hypothesis that fatal rabies may result from neuronal dysfunction rather than from structural damage (Tsiang, 1982).

Functional genomics and proteomics have been used to determine the host responses in cells or animals infected with different viruses (DeFilippis *et al*, 2003; Dhingra *et al*, 2005; Kellam, 2001), thus providing better understanding of pathogenic mechanisms by which virus infections lead to diseases. Previous genomic studies in our laboratory have demonstrated that wild-type (wt) RV evades the innate immune responses, thus contributing to pathogenicity (Wang *et al*, 2005). In the present study, we performed proteomic studies to profile protein expression in mice infected with wt or attenuated RV. It was found that infection with wt RV resulted in modulation of host proteins involved in ion homeostasis and synaptic physiology, which may provide structural and metabolic mechanisms by which RV infection causes neuronal dysfunction.

Results

Proteomic changes induced by RV infections

To further investigate how wt RV induces neurological diseases, we profiled host responses in mouse brain after infection with wt RV (SHBRV, silver-haired bat rabies virus) or attenuated B2C by two-dimensional (2D) gel analysis. Previous studies have demonstrated that SHBRV is more virulent than B2C in the mouse model (Wang *et al*, 2005). It was also found that B2C induced severe pathology including inflammation, gliosis, necrosis, and apoptosis, whereas very few histological changes were observed in mice infected with SHBRV (Sarmento *et al*, 2005). Brain samples were harvested from mice infected with 10 $ICLD_{50}$ of either virus (B2C or SHBRV) by the intracerebral (i.c.) route as described (Wang *et al*, 2005). At the time of severe paralysis, mice were sacrificed and brains removed and flash-frozen on dry ice before being stored at -80°C. Brain tissues were processed for 2D analysis as described (Dhingra *et al*, 2005). Figure 1 illustrates representative 2D electrophoresis images of protein profiles from mouse brains either sham-infected or infected with SHBRV or B2C. About 360 spots in each Sypro Ruby–stained gel were visualized by Dycyder software (data not shown). In comparison with the 2D electrophoresis profile from the healthy controls, many spots that may represent different degrees of protein modification and/or degradation products were found to be significantly expressed in mice infected with each RV strain.

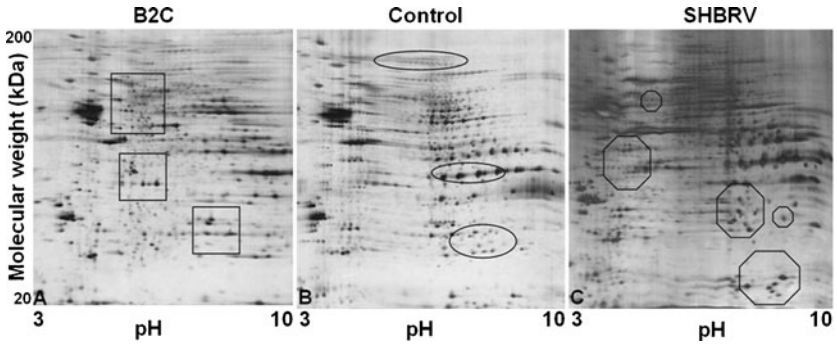

Figure 1 Representative 2D maps of proteins from sham-infected mouse brain and mouse brain infected with SHBRV or B2C. Brain proteins were analyzed by 2D gel electrophoresis. First dimension of the gel electrophoresis was carried out using immobilized pH gradient gel (pH 3 to 10) and second dimension of the electrophoresis is performed on 10% SDS-PAGE to separate proteins by molecular weight (20 to 200 kDa). The protein spots differentially expressed were marked by squares, ovals, or octagons, respectively, for B2C-, sham-, or SHBRV-infected mouse brain.

Table 1 Proteins differentially expressed in mice infected with SHBRV and B2C

Category	Protein	PI	Molecular weight (kDa)	Fold change	
				IC	IM
SHBRV					
Ion homeostasis	Na^+/K^+ ATPase	5.3	110	+3.0	+2.6
	H^+ ATPase subunit a isoform 1	6.0	96	+2.6	NK
Synaptic physiology	TRIM 9	6.6	90	−3.0	NK
	α-SNAP	5.3	33	−3.0	−2.0
	Pallidin (syntaxin 13)	5.8	20	−2.2	NK
	Synexin	5.9	50	−2.0	−2.4
	Syntaxin 18	5.2	35	−1.8	NK
Apoptosis	Caspase 1	5.7	45	−3.2	NK
	Annexin	5.4	45	NK	−2.2
	APAF 1	5.9	140	−3.0	NK
	Ras-GTPase–activating protein		68	−1.8	−2.2
Others	SAP 1	5.0	40	−2.8	NK
	CDC 42 (Rho family GTPase)	5.2	24	−2.2	NK
	Proteasome component 9	7.7	30	−1.8	NK
Unknown	Unknown-1	5.3	42	−3.6	NK
	Unknown-2	4.8	86	−2.2	NK
	Unknown-3	5.8	112	−2.0	NK
	Unknown-4	5.6	66	NK	−2.4
	Unknown-5	4.8	92	NK	+3.0
	Unknown-6	6.6	101	NK	+2.8
B2C					
Innate immunity	G protein–coupled receptor 44	4.8	88	+3	NK
	Hsp 60	5.9	60	+3.2	+3.6
	Hsp 70	4.8	70	NK	+2.1
Ion homeostasis	Villin 1	5.1	89	−2	NK
	Calretinin	4.9	31	−2.2	NK
	H^+ ATPase synthase subunit b	5.5	58	−2.8	−2.2
Apoptosis	APAF 1	6.0	143	+2.4	+2.8
	SH3 domain binding protein 2	7.6	62	+2.6	+2.8
Neurophysiology	Neurofilament protein NF 66	5.1	60	−3	NK
	CRMP-2	6.6	62	+3.6	NK
	α-Internexin	5.1	60	NK	−3.6
	Dihydropyrimidinase-related protein 1	6.6	63	NK	+2.8
Others	Trehalase	5.4	55	−2.4	NK
	Er-60 precursor	6.0	56	+3	NK
	Malate dehydrogenase	6.5	22	+2.1	NK
	Cathepsin	5.5	37	+2	NK
	Elongation factor-2	6.8	96	+2.5	+3.0
	Isocitrate dehydrogenase	5.7	68	NK	+3.2
	1110055E19Rik protein	6.7	45	NK	−2.6
Unknown	Unknown-1	5.2	42	+2.2	NK
	Unknown-2	5.6	48	+2	+2.4
	Unknown-3	6.6	63	−2.8	NK
	Unknown-4	6.8	112	−2.4	NK
	Unknown-5	7.2	115	−2	NK
	Unknown-6	5.4	66	NK	−1.8
	Unknown-7	6.2	86	NK	+2.4

Note. NK: not known; PI: isoelectric point.

Identification of differentially expressed proteins

Proteomics analysis of differentially expressed proteins among SHBRV-, B2C-, and sham-infected brain tissues showed that most of the protein spots were between 150 kDa and 20 kDa. Fifty-five protein spots were found to be significantly increased or decreased ($\geq$ twofold change) in infected brain tissue (B2C or SHBRV) when compared to sham-infected control. These 55 spots were excised, in-gel digested with trypsin, and analyzed by mass spectrometry (MS). The sequence coverage of the identified proteins by peptide mass fingerprinting ranges from 35% to 68%, depending on the size and amount of proteins. For protein spots with insufficient quantities, MS/MS was used to confirm protein identification. The up- or down-regulated proteins are summarized in Table 1.

Wild-type SHBRV and laborator-attenuated B2C differentially modulates the expression of host proteins

SHBRV and attenuated B2C viruses differentially modulated the expression of host proteins. In particular, SHBRV induced the expression of host proteins involved in ion homeostasis such as Na^+/K^+ ATPase and H^+ ATPase (also known as vacuolar ATP synthase), but down-regulated the expression

of several proteins relevant to synaptic physiology such as α-SNAP, syntaxin-18, tripartite motif protein (TRIM 9), and pallidin. In addition, SHBRV down-regulated the expression of proteins important in the induction of apoptosis such as caspase 1 and APAF-1. On the other hand, attenuated B2C induced the expression of proteins that play important roles in innate immune responses (G protein–coupled receptors and heat shock protein, HSP60) and in the induction of apoptosis (APAF-1), while down-regulating the expression of proteins involved in ion homeostasis (H^+ ATPase, calretinin) and neuronal morphogenesis (neurofilament 66). To validate the proteomics data, Western blotting was performed on selected proteins including synaptic proteins (Trim9, α-SNAP) and proteins involved in ion homeostasis (H^+ ATPase, Na^+/K^+ ATPase, Ca^{2+} ATPase). H^+ ATPase and Na^+/K^+ ATPase were up-regulated whereas Ca^{2+} ATPase was down-regulated in SHBRV-infected mouse brain (Figure 2A). In mice infected with B2C, H^+ ATPase and Na^+/K^+ ATPase were down-regulated whereas the expression of Ca^{2+} ATPase did not change. Synaptic proteins TRIM9 and α-SNAP were down-regulated in SHBRV-infected mice whereas infection with B2C did not change the expression level of these two proteins (Figure 2C). To confirm if RV infection also results in modulation of host protein expression in cultured cells, mouse primary cortical neurons prepared as described (Li *et al*, 2005) and infected with either B2C or SHBRV at 1 focus-forming unit (ffu) were subjected to Western blotting. As shown in Figure 2B, similar protein profile was obtained for the ATPases in infected neurons as seen in infected mice. The results from the Western blotting were comparable to the data obtained by 2D electrophoresis. The fold increase or decrease in mice infected with either SHBRV or B2C over the controls is similar for proteins in both proteomics data and Western blot results (Figure 2 and Table 1). To further confirm the proteomic profiling, mice were also infected with SHBRV and B2C by the intramuscular route and brains were removed for proteomic profiling. The available data are included in Table 1 and indicate that SHBRV and B2C modified the expression of similar proteins with comparable fold changes.

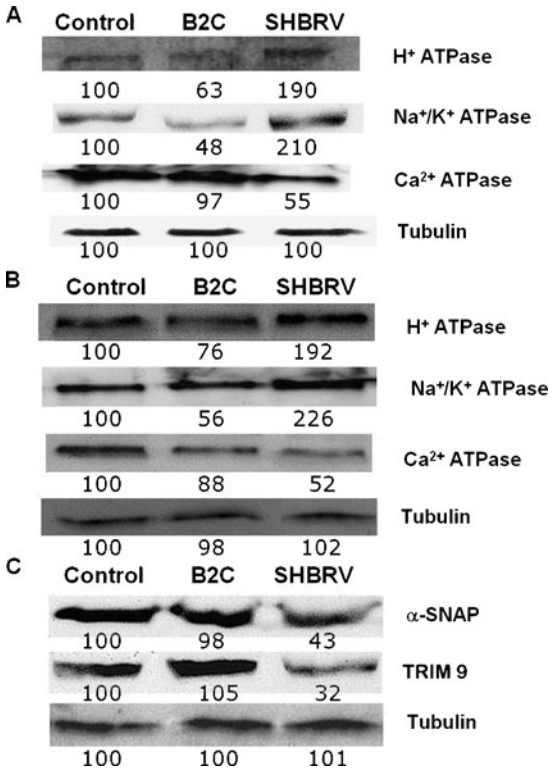

Figure 2 Western blot analysis of differentially expressed proteins. Proteins were extracted from mouse brains (**A** and **C**) or from primary neurons (**B**) and probed with antibodies to H^+ ATPase, Na^+/K^+ ATPase, or Ca^{2+} ATPase (**A** and **B**) or to α-SNAP and TRIM9 (**C**). Tubulin was used as a reference protein. Control, sham-infected mouse brain or neurons; B2C, mouse brain or neurons infected with B2C; SHBRV, mouse brain or neurons infected with SHBRV.

Immunohistochemistry was also performed to validate the proteomics data. Mice sham-infected or infected with either virus intracerebrally were perfused and brains removed for immunohistochemistry to measure the expression of Na^+/K^+ ATPase, Ca^{2+} ATPase, and α-SNAP. The expression of RV N was also measured. Figure 3 depicts the expression of these proteins in cerebral cortex and similar results were also obtained in other brain regions such as the brain stem and hippocampus (data not shown). Although the intensity of N expression is higher in mice infected with B2C than with SHBRV, almost all the neurons in the brain are infected by either virus. The expression of Na^+/K^+ ATPase increased in mice infected with SHBRV, but decreased in mice infected with B2C. On the other hand, the expression of Ca^{2+} ATPase and α-SNAP was reduced in mice infected with SHBRV, but not in sham-infected mice or mice infected with B2C, further confirming the proteomics data.

Changes in Na^+ and Ca^{2+} concentration in BSR cells following RV infection

To determine if modification of Na^+/K^+ ATPase or Ca^{2+} ATPase expression after RV infection results in changes of Na^+ and Ca^{2+} concentration, BSR cells were infected with RV (SHBRV or B2C) at 1 ffu per cell and Na^+ and Ca^{2+} concentrations measured at days 1, 3, and 5 after infection using cell-permeable forms of Sodium Green and Calcium Orange as the fluorescence indicator. All the cells are infected with each RV by day 3 post infection as detected by direct immunofluorescent assay (data not shown). Fluorescence intensity measurement showed that Na^+ concentration was significantly increased in cells infected with B2C, but decreased in cells infected with SHBRV (Figure 4, *top*) when compared with sham-infected controls. Ca^{2+} concentration was also significantly reduced in SHBRV-infected cells and it did not change in B2C-infected cells (Figure 4, *bottom*). To investigate the relationship between the level of

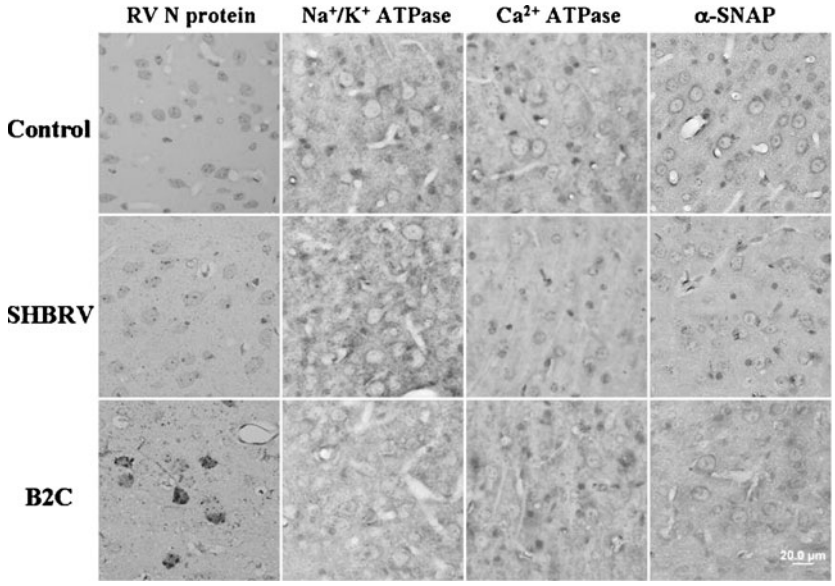

Figure 3 Immunohistochemical analysis of differentially expressed proteins. Mice were infected with 10 $ICLD_{50}$ of each virus and brains were harvested for immunohistochemistry for detection of viral antigen (RV N) and host protein (Na^+/K^+ ATPase, Ca^{2+} ATPase, or α-SNAP) using antibodies as described in Materials and Methods.

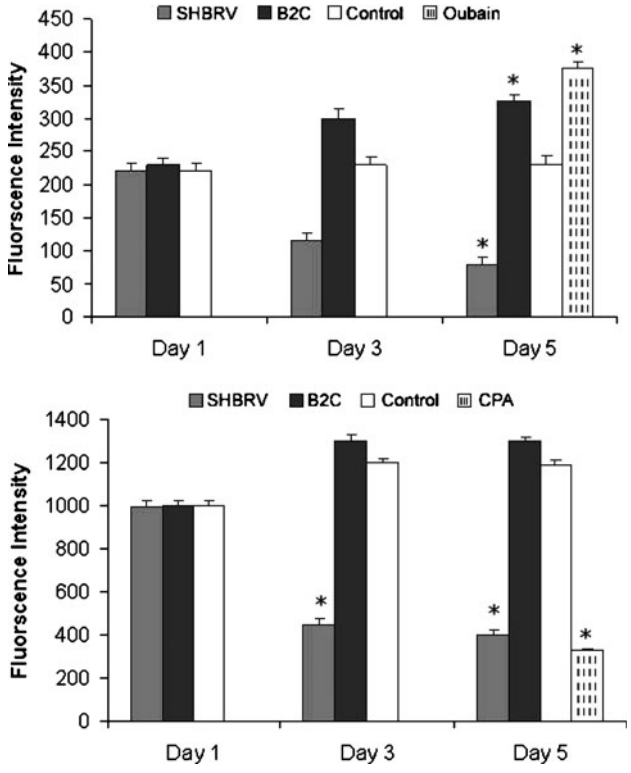

Figure 4 Intracellular Na^+ and Ca^{2+} concentrations in BSR cells. BSR cells sham-infected (control) or infected with B2C or SHBRV were treated with sodium green *(top)* or calcium orange *(bottom)*. At days 1, 3, and 5 after infection, fluorescence intensity was measured with a fluorimeter and the average fluorescence intensity from three replicas is depicted. Oubain and CPA were used as positive controls for Na^+/K^+ ATPase and Ca^{2+} ATPase inhibitors, respectively. *Significantly more Na^+ ($P < .01$) in B2C-infected cells and in cells treated with oubain, but significantly less in SHBRV-infected cells than in sham-infected cells as well as significantly less Ca^{2+} ($P < .01$) in SHBRV-infected BSR cells or cells treated with CPA than in sham-infected controls.

Na^+/K^+ ATPase and Ca^{2+} ATPase expression and the intracellular levels of Na^+ and Ca^{2+}, we used the known ATPase inhibitors ouabian (Na^+/K^+) and cyclopiazonic acid (CPA; Ca^{2+}). Inhibition of Na^+/K^+ ATPase led to the increase of Na^+ concentration and inhibition of Ca^{2+} ATPase resulted in decreased Ca^{2+} concentration (Figure 4).

Accumulation of synaptic vesicles in the presynaptic membrane of mice infected with SHBRV, but not in mice infected with B2C

Down-regulation of synaptic proteins such as syntaxin-18, α-SNAP, and TRIM 9 can result in blockade of synaptic vesicles to dock to and hence fuse with plasma membrane (Pozzo-Miller *et al*, 1999). To determine if down-regulation of synaptic proteins in mice infected with wt SHBRV leads to inhibition of synaptic vesicles docking and release, we performed electron microscopy (EM) on mouse brains infected with or without RV (2 mice in each group) as described (Li *et al*, 2005). In sham-infected mice, neurons in the hippocampus showed normal morphology with nuclei clearly demarcated and neuronal processes exhibit clear patterns with either transverse or longitudinal distributions (Figure 5A). Synapses and synaptic vesicles were clearly visible (Figure 5D). An average of 13 synaptic vesicles was observed per synapse (Figure 5G). In mice infected with B2C, normal neuronal morphology was no longer visible and nuclear blebbing was seen (early stage of apoptosis) (Figure 5B). The number of synapses and synaptic vesicles was reduced (Figure 5E) and only an average of eight synaptic vesicles were seen per synapse (Figure 5G). In SHBRV-infected mice, neuronal bodies showed recognizable morphology (Figure 5C). Synapses were enlarged

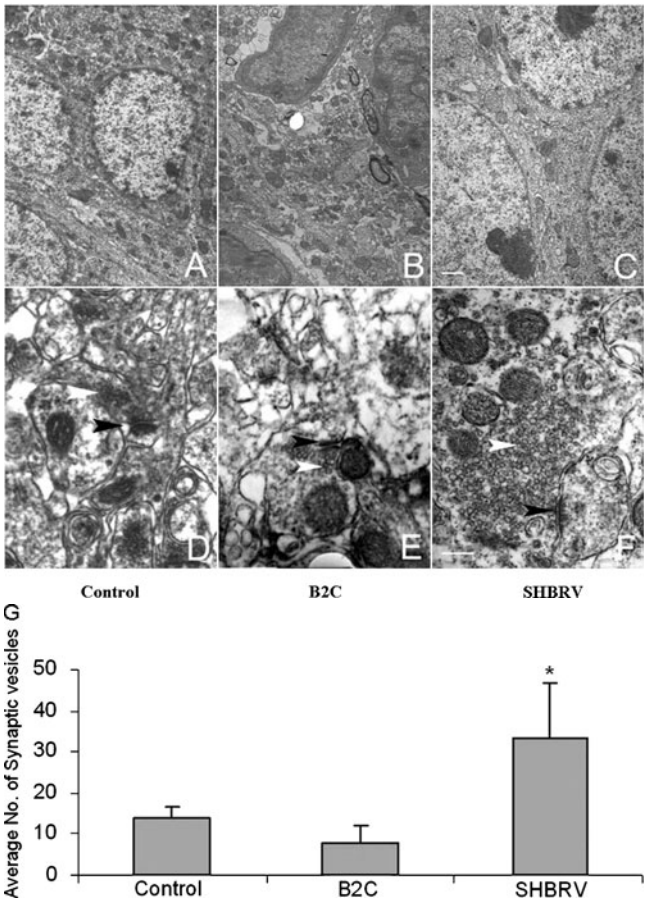

Figure 5 Ultrastructural changes of hippocampal neurons after infection with RV. Mice sham-infected or infected with B2C or SHBRV were perfused with 2.5% glutaraldehyde and 2% paraformaldehyde. Ultrathin sections were stained with uranium acetate/lead citrate, and examined under an electron microscope *(top)*. Sections **A, B,** and **C** show neuronal bodies and sections **D, E,** and **F** show synapses. Solid arrows and open arrowheads indicate for synapses and synaptic vesicles, respectively (**D, E,** and **F**). Scale bar, 1 μm (**A, B, C**); 250 nm (**D, E, F**). The average number of clustered synaptic vesicles at the synapses was quantified (**G**). Synaptic vesicles were counted in at least 10 synapses from each mouse and the average number of synaptic vesicles per synapse from sham-infected, B2C- and SHBRV-infected brains was used for statistical analysis by one-way ANOVA. *Significantly more synaptic vesicles in SHBRV-infected mouse brain than in sham-infected control ($P < .05$).

with significantly more synaptic vesicles (more than 30 per synapse) (Figure 5F and G). These ultrastructual studies demonstrate that down-regulation of synaptic proteins (syntaxin-18, α-SNAP, and TRIM 9) in SHBRV-infected mice resulted in inhibition of synaptic docking and fusion, leading to accumulation of synaptic vesicles in the presynaptic membrane.

Discussion

The proteomics technology is conceptually well suited to describe the molecular anatomy of a system and its changes in levels of protein and their expression pattern (Dhingra *et al*, 2005). Using 2D

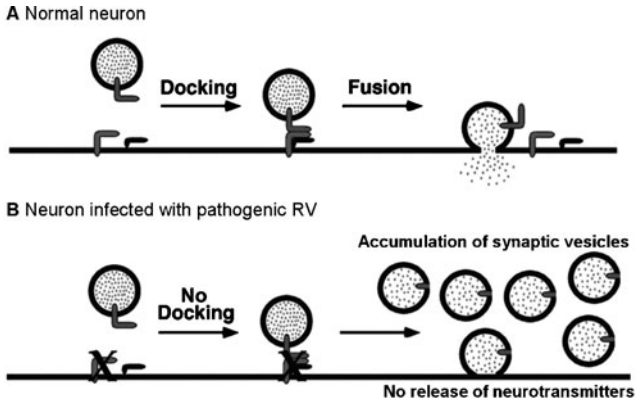

Figure 6 RV infection affects docking and fusing of synaptic vesicles and presynaptic membtrne, leading to accumulation of synaptic vesicles. In normal neurons, synaptic vesicles dock and fuse with presynaptic membrane, resulting in neurotransmitter release in the synapses (**A**). Pathogenic RV, by down-regulation of SNARE proteins, inhibits docking and fusing of synaptic vesicles, resulting in accumulation of synaptic vesicles in the presynapses (**B**).

gel electrophoresis coupled with Matrix Assisted Laser Desorption/Ionization Time-of-Flight (MALDI-TOF)/MS, we found that infection of mice with RV results in modulation of host protein expression. More than 55 proteins were found to be either up- or down-regulated following SHBRV or B2C infection. Most importantly, detailed analyses demonstrate that wt SHBRV induced changes in the expression of host proteins involved in ion homeostasis and in synaptic physiology in the CNS. H^+ ATPase and Na^+/K^+ ATPase were found to be up-regulated whereas Ca^{2+} ATPase and SNAREs such as α-SNAP, syntaxin-18, TRIM9, as well as pallidin were down-regulated in mice infected with wt SHBRV. Changes in the level of protein expression as detected by proteomics have been confirmed by Western blotting and immunohistochemistry. All these proteins with changes in expression play important roles in maintaining normal neuronal functions. Up- or down-regulation of these proteins, therefore, could lead to severe neuronal damages and dysfunctions.

Ion homeostasis plays important roles in the maintenance of transmembrane ionic concentration gradients, thus normal function of all animal cells (Mobasheri *et al*, 2000; Romero, 2004). Brain tissues are more sensitive to disruption of ion homeostasis than other tissues (Stys *et al*, 1992; Urenjak and Obrenovitch, 1996). Data from our proteomics analysis, Western blotting, and immunohistochemistry demonstrate that wt and attenuated RV differentially modulated the expression of Na^+/K^+ ATPase and Ca^{2+} ATPase. In mice infected with wt SHBRV, Na^+/K^+ ATPase was up-regulated but Ca^{2+} ATPase was down-regulated. Up-regulation of Na^+/K^+ ATPase is utilized to reduce Na^+ overload that can occur during muscle differentiation and intense contractions (Clausen, 1986). Indeed, increased expression of Na^+/K^+ ATPase resulted in reduced intracellular Na^+ concentrations significantly

in primary neurons infected with SHBRV as measured with cell-permeant Sodium Green (Friedman and Haddad, 1993). Intracellular Ca^{2+} concentrations were also reduced in neurons infected with SHBRV as a result of decreased expression of Ca^{2+} ATPase or due to enhanced Na^+/Ca^{2+} exchange following increased Na^+/K^+ ATPase (Duffy and MacVicar, 1996). Changes in Na^+ and Ca^{2+} concentration can lead to neuronal excitation and seizures (Somjen, 2002) and seizures are often observed in SHBRV-infected mice (Sarmento *et al*, 2005). On the other hand, Na^+/K^+ ATPase was down-regulated in B2C-infected mice or neurons and consequently increased Na^+ concentration was detected in B2C-infected cells. This observation is similar to those reported for Sindbis virus (Ulug *et al*, 1996). It has been reported that Sindbis virus E glycoprotein may be responsible for the inhibition of Na^+/K^+ ATPase (Despres *et al*, 1995). Persistent Na^+ accumulation due to reduction of Na^+/K^+ ATPase can induce intracellular edema and ischemic injury (Odland and Sutton, 1999; Urenjak and Obrenovitch, 1996). These data may partially explain why neuronal destruction is observed in B2C- but not in SHBRV-infected CNS (Sarmento *et al*, 2005).

Neuronal destruction observed in B2C-infected mice includes inflammation, necrosis, and apoptosis. However, neuronal destruction is minimal in mice infected with wt SHBRV (Sarmento *et al*, 2005), an observation similar to that reported in human patients (Murphy, 1977). Neuronal destruction such as inflammation and apoptosis has been proposed as a host protective response to clear virus-infected cells and thus a mechanism for RV attenuation (Morimoto *et al*, 1999; Sarmento *et al*, 2005; Wang *et al*, 2005; Yan *et al*, 2001). However, excessive neuronal destruction results in diseases and death (Sarmento *et al*, 2005). Infection with B2C induces apoptosis both *in vivo* and *in vitro* (Morimoto *et al*, 1999; Sarmento *et al*, 2005; Yan *et al*, 2001). The data from the present study provide some of the molecular mechanisms for the induction of apoptosis by B2C. Decrease in the level of Na^+/K^+ ATPase resulted in increased intracellular Na^+ concentration in B2C-infected cells, which can exacerbate swelling of cell body and axon, leading to apoptosis or a hybrid death consisted of apoptosis and necrosis in the same cell (Lynch *et al*, 1995; Stys, 1998). Increased intracellular Na^+ concentration also activates proteases like calpains (McGinnis *et al*, 1999), which can breakdown proteins that maintain axon structure (Araujo Couto *et al*, 2004). APAF1, a known marker for apoptosis by coupling mitochondria-released cytochrome *c* to activation of cytosolic caspases (Cecconi, 1999), was also found to be up-regulated in B2C-infecterd mice in this study as well as in our previous studies (Sarmento *et al*, 2006). The reduced expression of H^+ ATPase in B2C-infected cells may have a role to play in triggering apoptosis by inducing cellular acidosis (Ohta *et al*, 1996). Under EM, neurons from mice infected with B2C showed signs of apoptosis (nuclear blebbing and chromatin aggregation). On the other hand, the level of H^+ ATPase decreased in SHBRV-infected mice, which may represent a cellular antiapoptotic response (Gottlieb *et al*, 1995). Many of the apoptosis-inducing proteins such as caspase 1, APAF1, and ras-GTPase activation protein were found to be down-regulated in SHBRV-infected mice. All these data explain why apoptosis is only detected in animals or cells infected with attenuated RV, but not with wt SHBRV (Sarmento *et al*, 2005; Wang *et al*, 2005).

Another important finding in this study is that infection with wt SHBRV results in down-regulation of several proteins relevant to synaptic physiology such as α-SNAP, syntaxin-18, synexin, TRIM 9, and pallidin. These proteins are part of the so called SNAREs—proteins that are involved in all fusion competent membranes of the cell (Hong, 2005). Fusion cannot occur without SNAREs and is blocked when SNAREs are removed genetically or destroyed by neurotoxins (Lalli *et al*, 2003; Szule and Coorssen, 2003). Syntaxin-18, α-SNAP, and TRIM 9 are involved in docking of synaptic vesicles (Schiavo and Stenbeck, 1998) to the presynaptic membrane and thus play a key role in the release of neurotransmitters at the synapse (Hanson *et al*, 1997). Down-regulation of these proteins can therefore block the synaptic vesicles to dock and subsequently fuse to plasma membrane (Pozzo-Miller *et al*, 1999). Indeed, ultrastructural studies with EM revealed significantly more accumulation of synaptic vesicles in the presynaptic membrane in the CNS of mice infected with SHBRV than in mice sham-infected or infected with B2C. These data led us to hypothesize that pathogenic RV infection results in blockade of synaptic vesicles to dock at and/or fuse to the membrane and thus accumulation of synaptic vesicles in the presynapses, which may inhibit neurotransmitter release (see Figure 6). This could explain previous observations that RV infection resulted in reduced release and uptake of neurotransmitters (Fu and Jackson, 2005; Ladogana et al, 1994)

The data reported in this study further support our hypothesis that wt and laboratory-attenuated RVs induce neurological diseases and subsequent death by different mechanisms (Wang *et al*, 2005; Sarmento *et al*, 2005). Infection of mice with low doses of B2C induces mild apoptosis and inflammation in the spinal cord, preventing the virus from invading into the brain. However, infection with high doses of B2C resulted in activation of the innate immunity (Wang *et al*, 2005) and consequently extensive inflammation, necrosis and apoptosis in the CNS (Sarmento *et al*, 2005). These structural damages may play a role in encephalitis and death caused by attenuated RV. On the other hand, wt RV causes imbalance in ion homeostasis and down-regulation of SNARE proteins, which block the docking and fusion of synaptic vesicles to the presynaptic membrane, resulting in accumulation of presynaptic vesicles. These changes can lead to malfunction in neurotransmission. These alterations could trigger synaptic dysfunction and experimental demonstration is warranted.

Materials and methods

Animals, viruses, and other reagents

ICR mice (Harlan) at the age of 4 to 6 weeks were housed in temperature- and light-controlled quarters, with access to food and water *ad libitum*, in the Animal Facility, College of Veterinary Medicine, University of Georgia. Two RV strains were used in this study. One was the silver-haired bat RV (SHBRV), a street RV isolated from a human patient (Morimoto *et al*, 1996) and the other was the attenuated CVS-B2C, derived from the CVS-24 virus by passaging in BHK cells (Morimoto *et al*, 1998). Virus stocks were prepared as described (Yan *et al*, 2001) and stored at −80°C. *N*-Hydroxysuccinimide ester Cy3 and Cy5 dyes and Immobilised Dry-Strips (IPG strips) were purchased from GE Healthcare (Piscataway NJ). Sypro Ruby gel stain was purchased from Molecular Probes (Eugene, OR). Antibodies to Na^+/K^+ ATPase, Ca^{2+} ATPase, and H^+ ATPase were obtained from Chemicon. Anti-α-SNAP monoclonal antibody was purchased from Abcam, England. Anti-RV N antibodies were prepared as described previously (Wang *et al*, 2005). The Na^+/K^+ ATPase inhibitor (Ouabain) and Ca^{2+} ATPase inhibitor (cyclopiazonic acid; CPA) were purchased from Sigma-Aldrich (St Louis, USA). Complete mini protease inhibitor cocktail were from Boehringer (Mannheim, Germany).

Cell culture

BSR cells (derived from BHK cells) were cultured in Dulbecco's modified Eagle's medium (DMEM) supplemented with 10% fetal bovine serum, 100 units/ml penicillin, and 100 μg/ml streptomycin. Mouse primary neuronal cultures were prepared using standardized procedures as described (Li *et al*, 2005). Briefly, Swiss-Webster mice at gestation day 16 were euthanized and embryos were removed under sterile conditions. Neocortices from these embryos were collected and digested with trypsin. The separated neuronal cells were plated into culture wells treated with poly-D-lysine (50 μg/ml) and grown in MEM in a humidified atmosphere of 5% CO_2 at 37°C. Ara-C (cytosine furo-arabinoside) at 1 μM final concentration was added at 3 to 5 days after plating to prevent the proliferation of non-neuronal cells.

Animal infection and tissue collection

Mice were infected with 10 $ICLD_{50}$ of each virus (B2C or SHBRV) by the intracerebral (i.c.) or10 $IMLD_{50}$ of either virus by the intramuscular (i.m) route, as described (Wang *et al*, 2005). Infected animals were observed twice daily for 20 days for the development of rabies. At the time of severe paralysis, mice were sacrificed and brains removed and flash-frozen on dry ice before being stored at −80°C. For immunohistochemistry, mice were anesthetized with ketamine/xylazine at a dose of 0.2 ml and then perfused by intracardiac injection of phosphate-buffered saline (PBS) followed by 10% neutral buffered formalin as described (Yan *et al*, 2001). Brains were removed and placed in the same fixative (10% neutral-buffered formalin) for 1 week at 4°C. Tissues were paraffin embedded and coronal sections (4 μm) were obtained and placed on glass slides.

Sample preparation and labeling with cyanine dyes for 2D analysis

Brain tissues were processed for 2D analysis as described (Dhingra *et al*, 2005) by lysing in 7 M Urea containing 2 M thiourea, 10 mM dithiothreitol (DTT), 30 mM Tris, 4% CHAPS (3-[(3-cholamidopropyl) dimethylammonio]-1-propanesulfonate) and disrupted by ultrasonication (Braunsonic 300 s) on ice. The resulting homogenate was centrifuged twice for 30 min at 12,000 × *g* at 4°C. Protein concentration was measured by Bradford method using bovine serum albumin as a standard (Bradford, 1976). Protein lysates were labeled using the fluorescent cyanine dyes (Cy3 and Cy5) according to the manufacturer's protocols. Each protein lysate (50 μg) was labeled with 400 pmol of amine-reactive cyanine dyes, Cy3 or Cy5 *N*-hydroxysuccinamide (NHS) ester DIGE dyes (GE Healthcare), freshly dissolved in anhydrous dimethyl formamide. The labeling mixture was incubated on ice for 30 min in dark as described previously (Dhingra *et al*, 2005). The reaction was quenched by addition of 10 nmol of lysine (1/400 pmol dye) followed by incubation on ice for another 10 min.

Two-dimensional gel electrophoresis

The first dimension of gel electrophoresis was carried out using an immobilized pH gradient gel (immobilized dry strip) of pH 4 to 7 or pH 3 to 10 (Amersham Biosciences, GE Healthcare NJ). The strips were rehydrated in a rehydration solution containing 7 M Urea, 2 M thiourea, 2% CHAPS, 30 mM Tris, 2% IPG buffer, 28 mM DTT, and trace of bromophenol blue, overlaid with 3 ml dry strip cover fluid, in an immobiline dry strip reswelling tray. The samples were applied at the basic end of the IPG strip using a cup-loading technique. Isoelectric focusing (IEF) was carried out on a multiphor electrophoresis unit consisting of five phases of stepped voltages from 500 to 3500 V with total focusing of 48 kVh. Focusing started at 500 V for 4 h at 15°C and then continued at 3500 V for 12 h. The narrow pH range IPG strips were focused to 70 kVh. Prior to the second dimension, strips were equilibrated in buffer containing 6 M urea, 1% *w*/*v* sodium dodecyl sulfate (SDS), 30% *v*/*v* glycerol, 100 mM Tris, pH 6.8, reduced with 2% (*w*/*v*) DTT, and subsequently alkylated with 2.5% (*w*/*v*) iodoacetamide. After equilibration, proteins were separated on second-dimension separation on a 10% gel, 20 cm × 20 cm, at 30 mA constant. The gels were then stored in 1% acetic acid at 4°C until spot excision.

Protein visualization and image analysis
The Cy3 gel images were scanned on the Typhoon 9400 Variable Mode Imager (Amersham Biosciences) at an excitation wavelength of 540/25 nm (maxima/bandwidth) and at an emission wavelength of 590/30 nm, whereas the Cy5 gel images were scanned at an excitation wavelength of 620/30 nm and at an emission wavelength of 680/30 nm. Gel images were converted to 16-bit TIFF files and processed in DeCyder V3.0 (Amersham Biosciences). The spots on the gel were codetected automatically as DIGE image pairs, which were intrinsically linking a sample to its in-gel standard. Matching between gels was then performed utilizing the in-gel standard from each image pair. The experimental set up and relationship between samples were assigned in DeCyder, a 2D analysis software platform designed specially for DIGE. Each individual Cy5 gel image was assigned an experimental condition as either control or infected, and all Cy3 images were assigned as the standard.

Mass spectrometry
For peptide mass fingerprinting, in-gel digestion was either performed manually or by using an automated protein digestion system (Ettan digester; Amersham Biosciences) according to the manufacturer's protocol (Dhingra *et al*, 2005; Wait *et al*, 2001). In brief, the gel plugs were washed with 50 mM ammonium bicarbonate, then with 50% *v*/*v* acetonitrile in water followed by 100% *v*/*v* acetonitrile for dehydration. Following overnight digestion with trypsin in 50 mM ammonium bicarbonate (pH 8.0) at room temperature, peptides were extracted using sequential steps of 0.2% *v*/*v* Triflouro acetic acid (TFA) in water, followed by 50% *v*/*v* acetonitrile in 0.1% *v*/*v* TFA. The peptides were eluted with 5 μl of 50% *v*/*v* acetonitrile and 0.1% *v*/*v* TFA. The peptide extracts were used for MALDI-TOF protein identification (Henzel *et al*, 1993). The proteins used as controls were conalbumin type I, bovine serum albumin, carbonic anhydrase, trypsin inhibitor, and rabbit muscle glyceraldehydes 3-phosphate dehydrogenase (Bio-Rad). All standard proteins were identified in every run with >95% accuracy.

Analysis of peptide sequences
Peptide mass fingerprinting was used for protein identification using the measured monoisotopic masses of peptides and analyzed using the Mascot search engine (http://www.matrixscience.com), querying the masses in National Center for Biotechnology (NCBI) and SwissProt databases. A mass tolerance of 0.02 Da was used for masses measured in reflector mode and mass tolerance of 0.1% was used for masses measured in linear mode. Acetylation of the N-terminus, alkylation of cysteine, and oxidation of methionine were considered as possible modifications. Profound search engine (http://prowl. rockefeller.edu/profound bin/WebProFound.exe) was also used as a complementary and confirmatory search tool to the former.

Western blot analysis
For Western blotting, brain extracts as well as cell extracts were subjected to electrophoresis on a 10% polyacrylamide SDS gel (Laemmli, 1970). After separation on SDS-PAGE (polyacrylamide gel electrophoresis), proteins were electrotransferred to polyvinylidene difloride (PDVF) membrane blots. Then, blots were incubated with the respective antibody overnight at 4°C or for 2 h at room temperature. After three washes with PBST, blots were incubated for 1 h with horseradish peroxidase (HRP)–conjugated secondary antibody, followed by extensive washes in PBST. Proteins were detected by enhanced chemiluminescence (ECL; Amersham). Band signals corresponding to immunoreactive proteins were measured and scanned by image densitometry using Adobe Photoshop 6.0 software.

Immunohistochemistry
For immunohistochemistry, the procedure described by Yan *et al* (2001) was followed. Briefly, paraffin-embedded brain sections were heated at 70°C for 10 min, then dipped in Hemo-De for 3 × 5 min and dried until chalky white. Slides were incubated with proteinase K (20 μg/ml in 10 mM Tris-HCl, pH 7.4 to 8.0) for 15 min at 37°C and rinsed for 3 × 5 min with PBS. Tissue slides were incubated with antibodies (dilutions for antibodies to host proteins) to RV N or host proteins. The secondary antibody used was biotinylated goat anti-mouse or goat anti-rabbit immunoglobulin G (IgG) from the VectaStain kits (Vectorlab). The avidin-biotin-peroxidase complex (ABC) then was used to localize the biotinylated antibody. Finally diaminobenzidine (DAB) was used as a substrate for color development.

Measurements of intracellular sodium and calcium concentrations
To monitor changes of sodium and calcium concentrations in BSR cells infected with RV, cell-permeable forms of Sodium Green (Sodium Green tetra acetate) and Calcium Orange were used as the fluorescence indicator for Na^+ and Ca^{2+} in conjunction with fluorescence microscopy. The indicators were loaded into the cell for 30 min at room temperature and later washed with PBS. The fluorescence was monitored using the Zeiss LSM-510 microscope. Sodium Green and Calcium Orange fluorescence was also measured using a fluorimeter Synergy HT (Bio-Tek Instruments). The wavelengths of excitation/emission light of Sodium Green and Calcium Orange were 507/532 nm and 549/576 nm, respectively. Both sodium- (Sodium Green) and calcium- (Calcium Orange) specific fluorophores were from Molecular Probes (Eugene, OR).

The fluorophores were dissolved in dimethyl sulfoxide and stored at −20°C in the dark.

Electron microscopy (EM)
EM was performed as described (Li *et al*, 2005). Briefly, mice sham-infected or infected with SHBRV or B2C were transcardially perfused with 2.5% glutaraldehyde and 2% paraformaldehyde when the animals became moribund. After brain samples were harvested and embedded in Epon 812, the hippocampal areas were sectioned to semithin sections (1 μm). Then pyramid neurons and their processes were chosen to make ultrathin sections (0.3 to 0.4 μm) that were stained with uranium acetate-lead citrate and examined under a JEM-1210 electron microscope (Jeol, Japan).

References

Araujo Couto L, Sampaio Narciso M, Hokoc JN, Blanco Martinez AM (2004). Calpain inhibitor 2 prevents axonal degeneration of opossum optic nerve fibers. *J Neurosci Res* **77:** 410–419.

Bradford MM (1976). A rapid and sensitive method for the quantitation of microgram quantities of protein utilizing the principle of protein-dye binding. *Anal Biochem* **72:** 248–254.

Ceccaldi PE, Fillion MP, Ermine A, Tsiang H, Fillion G (1993). Rabies virus selectively alters 5-HT_1, receptor subtypes in rat brain. *Eur J Pharmacol* **245:** 129–138.

Cecconi F (1999). Apaf1 and the apoptotic machinery. *Cell Death Differ* **6:** 1087–1098.

Clausen T (1986). Regulation of active Na^+-K^+ transport in skeletal muscle. *Physiol Rev* **66:** 542–580.

DeFilippis V, Raggo C, Moses A, Fruh K (2003). Functional genomics in virology and antiviral drug discovery. *Trends Biotechnol* **21:** 452–457.

Despres P, Griffin JW, Griffin DE (1995). Antiviral activity of alpha interferon in Sindbis virus-infected cells is restored by anti-E2 monoclonal antibody treatment. *J Virol* **69:** 7345–7348.

Dhingra V, Li Q, Allison AB, Stallknecht DE, Fu ZF (2005). Proteomic profiling and neurodegeneration in west-nile-virus-infected neurons. *J. Biomed Biotech* **3:** 271–279.

Dietzschold B, Rupprecht CE, Fu ZF, Koprowski H (1996). Rhabdoviruses. In: *Fields virology*. Fields B, Knipe D, Howley PM (eds). New York: Raven Press, pp 1137–1159.

Duffy S, MacVicar BA (1996). In vitro ischemia promotes calcium influx and intracellular calcium release in hippocampal astrocytes. *J Neurosci* **16:** 71–81.

Etessami R, Conzelmann KK, Fadai-Ghotbi B, Natelson B, Tsiang H, Ceccaldi PE (2000). Spread and pathogenic characteristics of a G-deficient rabies virus recombinant: an in vitro and in vivo study. *J Gen Virol* **81:** 2147–2153.

Friedman JE, Haddad GG (1993). Major differences in Ca^{2+} response to anoxia between neonatal and adult rat CA1 neurones: role of Ca^{2+} and Na^+. *J Neurosci* **13:** 63–72.

Fu ZF, Jackson AC (2005). Neuronal dysfunction and death in rabies virus infection. *J NeuroVirol* **11:** 101–106.

Gottlieb RA, Giesing HA, Zhu JY, Engler RL, Babior BM (1995). Cell acidification in apoptosis: granulocyte colony-stimulating factor delays programmed cell death in neutrophils by up-regulating the vacuolar H(+)-ATPase, *Proc Natl Acad Sci USA* **92:** 5965–5968.

Gourmelon P, Briet D, Clarencon D, Court L, Tsiang H (1991). Sleep alterations in experimental street rabies virus infection occur in the absence of major EEG abnormalities. *Brain Res* **554:** 159–165.

Gourmelon P, Briet D, Court L, Tsiang H (1986). Electrophysiological and sleep alterations in experimental mouse rabies. *Brain Res* **398:** 128–140.

Hanson PI, Heuser JE, Jahn R (1997). Neurotransmitter release—4 years of SNARE complexes. *Curr. Opin. Neurobiol.* **9:** 310–315.

Hemachudha T (1994). Human rabies: clinical aspects, pathogenesis, and potential therapy. *Curr Top Microbiol Immunol.* **187:** 121–143.

Henzel WJ, Billeci TM, Stults JT, Wong SC, Grimley C, Watanabe C (1993). Identifying proteins from two dimensional gels by molecular mass searching of peptide fragments in protein sequence databases. *Proc Natl Acad Sci USA.* 90: 5011–5015.

Hong W (2005). SNAREs and traffic. *Biochim Biophys Acta* **1744:** 493–517.

Iwasaki Y, Tobita M (2002). Pathology In: *Rabies*. Jackson AC, Wunner WH (eds.). San Diego: Academic Press, pp 283–306.

Jackson AC (2003). Rabies virus infection: an update. *J NeuroVirol* **9:** 253–258.

Juntrakul S, Ruangvejvorachai P, Shuangshoti S, Wacharapluesadee S, Hemachudha T. (2005). Mechanisms of escape phenomenon of spinal cord and brainstem in human rabies. *BMC Infect Dis* **5:** 104.

Kellam P (2001). Post-genomic virology: the impact of bioinformatics, microarrays and proteomics on investigating host and pathogen interactions. *Rev Med Virol* **11:** 313–329.

Ladogana A, Bouzamondo E, Pocchiari M, Tsiang H (1994). Modification of tritiated gamma-amino-n-butyric acid transport in rabies virus-infected primary cortical cultures. *J Gen Virol* **75:** 623–627.

Laemmli UK (1970). Cleavage of structural proteins during the assembly of the head of bacteriophage T4. *Nature* **227:** 680–685.

Lalli G, Bohnert S, Deinhardt K, Verastegui C, Schiavo G (2003). The journey of tetanus and botulinum neurotoxins in neurons. *Trends Microbiol* **11:** 431–437.

Lentz TL, Burrage TG, Smith AL, Crick J and Tignor GH (1982). Is the acetylcholine receptor a rabies virus receptor? *Science* **215:** 182–184.

Li X, Samento L, Fu ZF (2005). Degenerative changes of mouse neuronal processes after rabies infection. *J Virol* **79:** 10063–10068.

Lynch JJ, Yu SP, Canzoniero LM, Sensi SL, Choi DW (1995). Sodium channel blockers reduce oxygen-glucose deprivation-induced cortical neuronal injury when combined with glutamate receptor antagonists. *J Pharmacol Exp Ther* **273:** 554–560.

McGinnis KM, Wang KK, Gnegy ME (1999). Alterations of extracellular calcium elicit selective modes of cell death

and protease activation in SH-SY5Y human neuroblastoma cells. *J Neurochem* **72:** 1853–1863.

Mitrabhakdi E, Shuangshoti S, Wannakrairot P, Lewis RA, Susuki K, Laothamatas J, Hemachudha T (2005). Difference in neuropathogenetic mechanisms in human furious and paralytic rabies. *J Neurol Sci* **238:** 3–10.

Mobasheri A, Avila J, Cozar-Castellano I, Brownleader MD, Trevan M, Francis MJ, Lamb JF, Martin-Vasallo P (2000). Na^+, K^+-ATPase isozyme diversity; comparative biochemistry and physiological implications of novel functional interactions. *Biosci Rep* **20:** 51–91.

Morimoto, K, Hooper DC, Carbaugh H, Fu ZF, Koprowski H, Dietzschold B (1998). Rabies virus quasispecies: implications for pathogenesis. *Proc Natl Acad Sci USA* **95:** 3152–3156.

Morimoto K, Hooper DC, Spitsin S, Koprowski H, Dietzschold B (1999). Pathogenicity of different rabies virus variants inversely correlates with apoptosis and rabies virus glycoprotein expression in infected primary neuron cultures. *J Virol.* **73:** 510–518.

Morimoto K, Patel M, Corisdeo S, Hooper DC, Fu ZF, Rupprecht CE, Koprowski H, Dietzschold B (1996). Characterization of a unique variant of bat rabies virus responsible for newly emerging human cases in North America. *Proc Natl Acad Sci USA* **93:** 5653–5658.

Muller EE, Nistico G (1988). *Brain messengers and the pituitary*. New York: Academic Press, New York.

Murphy FA, Bauer SP (1974). Early street rabies virus infection in striated muscle and later progression to the central nervous system. *Intervirology* **3:** 256–268.

Murphy FA (1977). Rabies pathogenesis. *Arch Virol* **54:** 279–297.

Odland RM, Sutton RL (1999). Hyperosmosis of cerebral injury. *Neurol Res* **21:** 500–508.

Ohta T, Arakawa H, Futagami F, Fushida S, Kitagawa H, Kayahara M, Nagakawa T, Miyazaki I, Numata M, Ohkuma S (1996). A new strategy for the therapy of pancreatic cancer by proton pump inhibitor. *Gan To Kagaku Ryoho* **23:** 1660–1664.

Pozzo-Miller LD, Gottschalk W, Zhang L, McDermott K, Du J, Gopalakrishnan R, Oho C, Sheng ZH, Lu B (1999). Impairments in high-frequency transmission, synaptic vesicle docking, and synaptic protein distribution in the hippocampus of BDNF knockout mice. *J Neurosci* **19:** 4972–4983.

Romero MF (2004). In the beginning, there was the cell: cellular homeostasis. *Adv Physiol Educ* **28:** 135–138.

Shankar V, Dietzschold B, Koprowski H (1991). Direct entry of rabies virus into the central nervous system without prior local replication. *J Virol* **65:** 2736–2738.

Sarmento L, Li XQ, Howerth E, Jackson AC, Fu ZF (2005). Glycoprotein-mediated induction of apoptosis limits the spread of attenuated rabies viruses in the central nervous system of mice. *J NeuroVirol* **11:** 571–581.

Sarmento L, Tseggai T, Dhingra V, Fu ZF (2006). Rabies virus-induced apoptosis involves caspase-dependent and caspase-independent pathways. *Virus Res* **121:** 144–151.

Schiavo G, Stenbeck G (1998). Molecular analysis of neurotransmitter release. *Essays Biochem* **33:** 29–41.

Somjen GG (2002). Ion regulation in the brain: implications for pathophysiology. *Neuroscientist* **8:** 254–267.

Stys PK (1998). Anoxic and ischemic injury of myelinated axons in CNS white matter: from mechanistic concepts to therapeutics. *J Cereb Blood Flow Metab* **18:** 2–25.

Stys PK, Waxman SG, Ransom BR (1992). Ionic mechanisms of anoxic injury in mammalian CNS white matter: role of Na^+ channels and Na^+-Ca^{2+} exchanger. *J Neurosci* **12:** 430–439.

Szule JA, Coorssen JR (2003). Revisiting the role of SNAREs in exocytosis and membrane fusion. *Biochim Biophys Acta* **1641:** 121–135.

Thoulouze MI, Lafage M, Schachner M, Hartmann U, Cremer H, Lafon M (1998). The neural cell adhesion molecule is a receptor for rabies virus. *J Virol* **72:** 7181–7190.

Tirawatnpong S, Hemachudha T, Manutsathit S, Shuangshoti S, Phanthumchinda K, Phanuphak P (1989). Regional distribution of rabies viral antigen in central nervous system of human encephalitic and paralytic rabies. *J Neurol Sci* **92:** 91–99.

Tuffereau C, Benejean J, Blondel D, Kieffer B, Flamand A (1998). Low-affinity nerve-growth factor receptor (P75NTR) can serve as a receptor for rabies virus. *EMBO J* **17:** 7250–7259.

Tsiang H (1982). Neuronal function impairment in rabies-infected rat brain. *J Gen Virol* **61:** 277–281.

Ulug ET, Garry RF, Bose HR (1996). Inhibition of Na^+K^+ATPase activity in membranes of Sindbis virus-infected chick cells. *Virology* **216:** 299–308.

Urenjak J, Obrenovitch TP (1996). Pharmacological modulation of voltage-gated Na^+ channels: a rational and effective strategy against ischemic brain damage. *Pharmacol Rev* **48:** 21–67.

Wait R, Gianazza E, Eberini I (2001). Proteins of rat serum, urine, and cerebrospinal fluid. VI. Further protein identifications and interstrain comparison. *Electrophoresis* **22:** 3043–3052.

Wang ZW, Sarmento L, Wang Y, Li XQ, Dhingra V, Tseggai T, Jiang B, Fu ZF (2005). Attenuated rabies virus activates, while pathogenic rabies virus evades, the host innate immune responses in the central nervous system. *J Virol* **79:** 12554–12565.

Yan X, Prosniak M, Curtis MT, Weiss ML, Faber M, Dietzschold B, Fu ZF (2001). Pathogenicity of different rabies virus variants inversely correlates with apoptosis and rabies virus glycoprotein expression in infected primary neuron cultures. *J NeuroVirol* **7:** 518–527.